

Photo catalytic reduction of carbon dioxide to methanol using a $\text{Bi}_2\text{WO}_6 @ \text{g-C}_3\text{N}_4$ nano composite

I.A. Mkhaliid

Department of Chemistry, Faculty of Science, King Abdulaziz University, PO Box 80203, 21589 Jeddah, Saudi Arabia, email: imkhalid2@gmail.com

Received 22 October 2017; Accepted 6 February 2018

ABSTRACT

Graphitic carbon nitride absorbs light in the visible region, but the electron-hole recombination rate is very fast. Decreasing the electron-hole recombination rate is very important in order to attain high efficiency. In this paper, this goal was achieved by the decoration of graphitic carbon nitride with Bi_2WO_6 . $\text{Bi}_2\text{WO}_6 @ \text{g-C}_3\text{N}_4$ and $\text{g-C}_3\text{N}_4$ were prepared using a hydrothermal method in the presence of octadecyltrimethyl ammonium bromide as a surfactant. The prepared materials were characterized by many techniques. The photo catalytic activity of $\text{Bi}_2\text{WO}_6 @ \text{g-C}_3\text{N}_4$ is 1.9 times better than $\text{g-C}_3\text{N}_4$ at methanol production. In addition, $\text{Bi}_2\text{WO}_6 @ \text{g-C}_3\text{N}_4$ exhibits photo catalytic stability for methanol production, which enables many reuses of the photo catalyst.

Keywords: $\text{g-C}_3\text{N}_4$; Bi_2WO_6 ; Carbon dioxide; Methanol

1. Introduction

Photo catalysis has attracted interest in many fields of scientific research and industrial applications. In photo catalysis, a catalyst is used in reactions under illumination of ultraviolet (uv) or visible radiation. Graphitic-carbon nitride ($\text{g-C}_3\text{N}_4$) has a sheet-like structure similar to that of graphite. This type of C_3N_4 structure has attracted researchers' attention in the field of photo catalysis because of its favorable properties, which include a narrow band gap, non-metallic structure, physical and chemical stability, and bio compatibility [1]. However, the high recombination rate of the electron-hole pair and the poor visible light harvesting hinders its efficiency as a photo catalyst [1,2]. Researchers often try to prepare $\text{g-C}_3\text{N}_4$ then decorate or dope it with an element or a group with the aim to reduce the recombination rate of the electron-hole pair and enhance visible light harvesting. Examples are abundant in the literature, for instance, TiO_2 has been used to improve the properties of $\text{g-C}_3\text{N}_4$ [3–6]. Metals and combinations of metals such

as Zn and its compounds [7–9], Fe [1,10,11], W [12,13], Sn [14], Ni [15], and Cr [16] have been added to $\text{g-C}_3\text{N}_4$ to improve its photo catalytic efficiency. Silver has been added to $\text{g-C}_3\text{N}_4$ not only to improve the properties but also to add a new dimension in the applications of antibacterial activity [17–20]. Non-metals such as graphene oxide and others were also added to $\text{g-C}_3\text{N}_4$ [21].

In this work, I report a new composite in which Bi_2WO_6 decorates $\text{g-C}_3\text{N}_4$ that was synthesized and characterized. In the preparation method, we used octadecyltrimethyl ammonium bromide as a surfactant for the first time in these types of syntheses. As an application of the synthesized material, the visible-light photo catalytic reduction of carbon dioxide using $\text{Bi}_2\text{WO}_6 @ \text{g-C}_3\text{N}_4$ was studied.

2. Experimental

2.1. Preparation of photo catalysts

In this procedure, two mixtures (A and B) were prepared. Mixture A: 5 g of octadecyltrimethyl ammonium bromide (OTAB) was dissolved in 20 mL of distilled water

*Corresponding author.

under magnetic stirring. Then, 0.01 M of urea was added to OTAB solution drop wise. Mixture B: $\text{Bi}(\text{NO}_3)_3 \cdot \text{H}_2\text{O}$ and $\text{Na}_2\text{WO}_4 \cdot 2\text{H}_2\text{O}$ were dissolved in 50 mL of bidistilled water under magnetic stirring. To prepare composites of various wt% of Bi_2WO_6 , namely, 0.5, 1.0, 1.5, and 2.0, stoichiometric amounts of these materials were added each time to prepare the four solutions.

To complete the synthesis of the decorated nanocomposite, Mixture A was added drop wise to mixture B, after which the resulting mixture was transferred to a Teflon-lined stainless steel autoclave and heated for 10 h at 200°C. The produced material was separated, washed many times and dried in an oven at 100°C for 12 h. To prepare $\text{g-C}_3\text{N}_4$, mixture A was transferred to a Teflon-lined stainless steel autoclave and heated for 10 h at 200°C, then the product material was separated, washed many times and dried in an oven at 100°C for 12 h.

2.2. Characterization

Powder X-ray diffraction (XRD) patterns were recorded with a Bruker axis D8 with $\text{CuK}\alpha$ radiation ($\lambda = 1.5418 \text{ \AA}$). The accelerating voltage and the emission current were 40 kV and 35 mA, respectively. Data were obtained over the 2θ range of 5–80°, with a step width of 0.02° and a scan rate of 5° min^{-1} . The ultraviolet-visible (UV-Vis) spectroscopy measurement was carried out on a UV-Vis-NIR spectrophotometer (V-570, Jasco, Japan), using BaSO_4 as the reference standard. Photoluminescence (PL) spectra were measured using a Shimadzu RF-5301 fluorescence spectrophotometer at room temperature, with the excitation light of 350 nm from a xenon lamp. The transmission electron microscopy (TEM) investigation was performed with a JEOL-JEM-1230 transmission electron microscope. The specific surface area was measured by using a Nova 2000 series Chromatech apparatus and calculated by the Brunauer-Emmett-Teller (BET) equation. A Thermo Scientific K-ALPHA spectrometer was utilized to obtain X-ray photo electron spectroscopy (XPS) measurements.

2.3. Photo catalytic tests

The photo catalytic performance was studied for the photo catalytic reduction of CO_2 under visible light. First, the required dose of the photo catalyst was dispersed in 50 mL of 0.08 M sodium bicarbonate solution. The dimensions of the reactor used are 30 cm \times 15 cm \times 5 cm. To remove oxygen from the reaction mixture, nitrogen gas was bubbled through the reaction mixture for 1 h. To obtain adsorption-desorption equilibrium, the reaction mixture was stored in the dark for 30 min. Then, a 500 W high-pressure Xe lamp was used as a source of irradiation, and we used 2 M NaNO_2 solution to cut off the UV region below 400 nm. The obtained methanol was analyzed using GC-FID. The yield of evolved methanol can be calculated by dividing the total amount of methanol evolved by the reaction time. There was no methanol detected for all tested samples when the reaction was carried out in the dark only. Also, there was no methanol detected for all tested samples when the reaction was carried out using the source of irradiation only.

3. Results & discussion

3.1. Characterizations of materials

Fig. 1. shows XRD patterns of the five synthesized composites, $\text{g-C}_3\text{N}_4$, 0.5 wt % $\text{Bi}_2\text{WO}_6 @ \text{g-C}_3\text{N}_4$, 1.0 wt % $\text{Bi}_2\text{WO}_6 @ \text{g-C}_3\text{N}_4$, 1.5 wt % $\text{Bi}_2\text{WO}_6 @ \text{g-C}_3\text{N}_4$ and 2.0 wt % $\text{Bi}_2\text{WO}_6 @ \text{g-C}_3\text{N}_4$. The patterns reveal the pure $\text{g-C}_3\text{N}_4$ phase in all five composites with no peaks of Bi_2WO_6 , which could be explained by the low percentage of Bi_2WO_6 that was present. The patterns also show there is no shift in peaks of $\text{g-C}_3\text{N}_4$, which means successful decoration of $\text{g-C}_3\text{N}_4$ by Bi_2WO_6 . The crystallite sizes of $\text{g-C}_3\text{N}_4$, 0.5 wt % $\text{Bi}_2\text{WO}_6 @ \text{g-C}_3\text{N}_4$, 1.0 wt % $\text{Bi}_2\text{WO}_6 @ \text{g-C}_3\text{N}_4$, 1.5 wt % $\text{Bi}_2\text{WO}_6 @ \text{g-C}_3\text{N}_4$ and 2.0 wt % $\text{Bi}_2\text{WO}_6 @ \text{g-C}_3\text{N}_4$ are 16, 14, 12, 10 and 9 nm, respectively, as calculated by the Scherrer formula. It is clear that Bi_2WO_6 doping results in a decrease of crystallite sizes of $\text{g-C}_3\text{N}_4$. This may be due to the addition of Bi_2WO_6 to $\text{g-C}_3\text{N}_4$ preventing the growth of $\text{g-C}_3\text{N}_4$ and thereby decreasing its crystallinity and size.

Fig. 2 shows TEM images of $\text{g-C}_3\text{N}_4$, 0.5 wt % $\text{Bi}_2\text{WO}_6 @ \text{g-C}_3\text{N}_4$, 1.0 wt % $\text{Bi}_2\text{WO}_6 @ \text{g-C}_3\text{N}_4$, 1.5 wt % $\text{Bi}_2\text{WO}_6 @ \text{g-C}_3\text{N}_4$ and 2.0 wt % $\text{Bi}_2\text{WO}_6 @ \text{g-C}_3\text{N}_4$. The results reveal that the decoration and dispersion of Bi_2WO_6 above the surface of $\text{g-C}_3\text{N}_4$ were increased by increasing the weight percent of Bi_2WO_6 from 0 to 1.5 wt %, while the dispersion was decreased above 1.5 wt %. The 1.5 wt % $\text{Bi}_2\text{WO}_6 @ \text{g-C}_3\text{N}_4$ sample was measured by HRTEM as shown in Fig. 2 F. The presence of lattice spacing at 0.315 nm and 323 nm confirm the presence of Bi_2WO_6 phase (113) and $\text{g-C}_3\text{N}_4$ phase (002) for the 1.5 wt % $\text{Bi}_2\text{WO}_6 @ \text{g-C}_3\text{N}_4$ sample, respectively, as shown in Fig. 2F.

Fig. 3 shows XPS spectra of Bi4f, O1s, W4f, C1s and N1s species for the 1.5 wt % $\text{Bi}_2\text{WO}_6 @ \text{g-C}_3\text{N}_4$ sample. It shows two peaks for Bi4f_{7/2} and Bi4f_{5/2} at 158.2 and 163.4 eV, respectively confirming the bismuth ion (Bi^{3+} ion) as shown in Fig. 3A. Fig. 3B shows one peak for O1s at 529.1 eV, confirming the oxygen ion (O^{2-} ion). Fig. 3C shows two

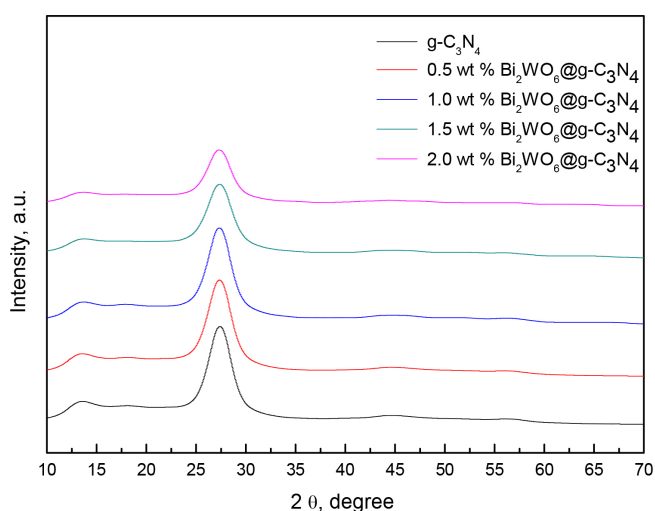


Fig. 1. XRD patterns of $\text{g-C}_3\text{N}_4$, 0.5 wt % $\text{Bi}_2\text{WO}_6 @ \text{g-C}_3\text{N}_4$, 1.0 wt % $\text{Bi}_2\text{WO}_6 @ \text{g-C}_3\text{N}_4$, 1.5 wt % $\text{Bi}_2\text{WO}_6 @ \text{g-C}_3\text{N}_4$ and 2.0 wt % $\text{Bi}_2\text{WO}_6 @ \text{g-C}_3\text{N}_4$ samples.

peaks for $W4f_{7/2}$ and $W4f_{5/2}$ at 34.4 and 36.5 eV, respectively, confirming the tungsten ion (W^{6+} ion). The results from Figs. 3A–3C confirm the presence of Bi_2WO_6 in the nanocomposite structure. Fig. 3D shows two peaks for C1s at 287.6 and 284.5 eV, confirming the carbon ion (C=N). Fig. 3E shows one peak for N1s at 399.0 eV, confirming the nitrogen ion (C=N-C). The results from Figs. 3D and 3E confirm the presence of $g-C_3N_4$ in the nanocomposite structure. Therefore, the nanocomposite structure is $Bi_2WO_6@g-C_3N_4$.

The specific surface area of $g-C_3N_4$, 0.5 wt % $Bi_2WO_6@g-C_3N_4$, 1.0 wt % $Bi_2WO_6@g-C_3N_4$, 1.5 wt % $Bi_2WO_6@g-C_3N_4$

and 2.0 wt % $Bi_2WO_6@g-C_3N_4$ samples was measured by a Nova 2000, resulting in values of 70, 69.8, 69.7, 69.6 and 69.5 m^2/g , respectively, as shown in Table 1. Therefore, the addition of Bi_2WO_6 to $g-C_3N_4$ had no significant effect on the BET surface area of $g-C_3N_4$.

UV-Vis spectra of $g-C_3N_4$, 0.5 wt % $Bi_2WO_6@g-C_3N_4$, 1.0 wt % $Bi_2WO_6@g-C_3N_4$, 1.5 wt % $Bi_2WO_6@g-C_3N_4$ and 2.0 wt % $Bi_2WO_6@g-C_3N_4$ samples (Fig. 4) reveal a red shift of absorption edges of $g-C_3N_4$ toward higher wavelengths going from 0.5 to 2.0 wt % from Bi_2WO_6 . The values of band gap energy of $g-C_3N_4$, 0.5 wt % $Bi_2WO_6@g-C_3N_4$, 1.0 wt % $Bi_2WO_6@g-C_3N_4$, 1.5 wt % $Bi_2WO_6@g-C_3N_4$ and 2.0 wt %

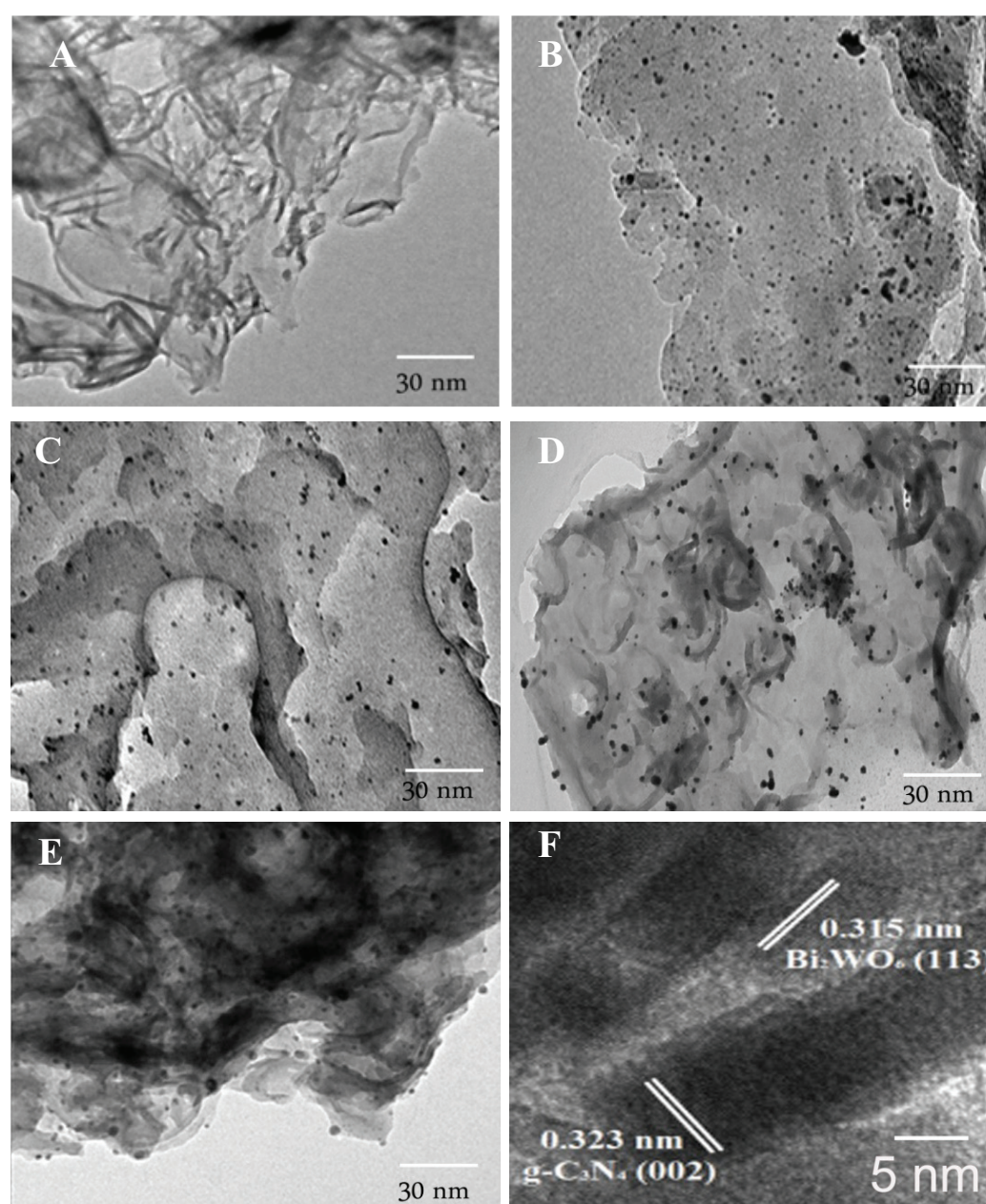


Fig. 2. TEM images of $g-C_3N_4$ (A), 0.5 wt % $Bi_2WO_6@g-C_3N_4$ (B), 1.0 wt % $Bi_2WO_6@g-C_3N_4$ (C), 1.5 wt % $Bi_2WO_6@g-C_3N_4$ (D), 2.0 wt % $Bi_2WO_6@g-C_3N_4$ (E) and the HRTEM image for 1.5 wt % $Bi_2WO_6@g-C_3N_4$ (F).

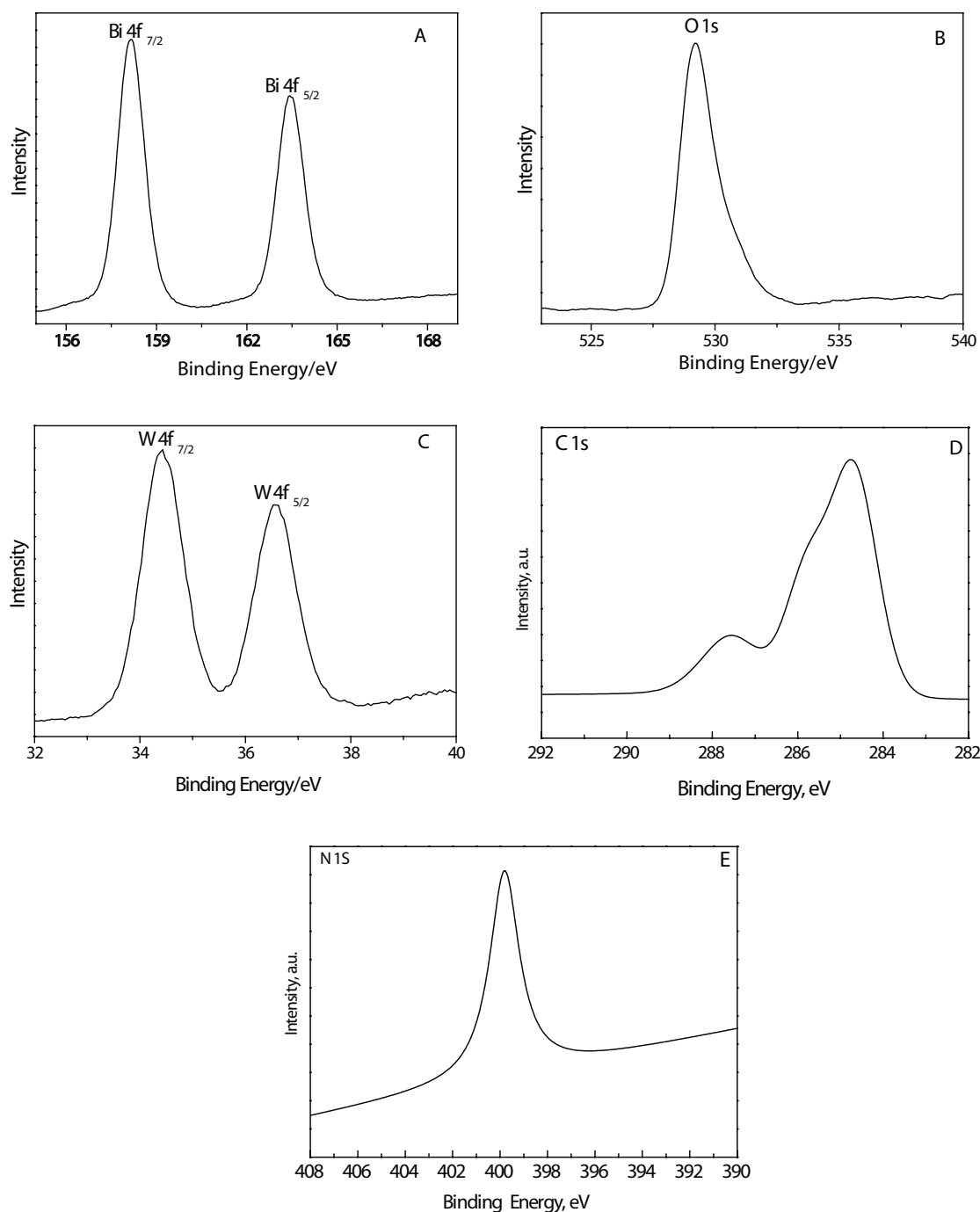


Fig. 3. XPS spectra of XPS spectra of Bi4f (A), O1s (B), W4f (C), C1s (D) and N1s (E) species for the 1.5 wt % $\text{Bi}_2\text{WO}_6@ \text{g-C}_3\text{N}_4$ sample.

Table 1
BET surface area of $\text{g-C}_3\text{N}_4$ and $\text{Bi}_2\text{WO}_6@ \text{g-C}_3\text{N}_4$ samples

Samples	Surface area (m^2/g)
$\text{g-C}_3\text{N}_4$	70
0.5 wt % $\text{Bi}_2\text{WO}_6@ \text{g-C}_3\text{N}_4$	69.8
1.0 wt % $\text{Bi}_2\text{WO}_6@ \text{g-C}_3\text{N}_4$	69.7
1.5 wt % $\text{Bi}_2\text{WO}_6@ \text{g-C}_3\text{N}_4$	69.6
2.0 wt % $\text{Bi}_2\text{WO}_6@ \text{g-C}_3\text{N}_4$	69.5

$\text{Bi}_2\text{WO}_6@ \text{g-C}_3\text{N}_4$ samples calculated from their respective UV-Vis spectra were 2.43, 2.27, 2.25, 2.02 and 2.01 eV, respectively, as shown in Table 2. These results indicate narrowing of the band gap, and therefore higher visible light photo catalysis efficiency.

PL spectra of $\text{g-C}_3\text{N}_4$, 0.5 wt % $\text{Bi}_2\text{WO}_6@ \text{g-C}_3\text{N}_4$, 1.0 wt % $\text{Bi}_2\text{WO}_6@ \text{g-C}_3\text{N}_4$, 1.5 wt % $\text{Bi}_2\text{WO}_6@ \text{g-C}_3\text{N}_4$ and 2.0 wt % $\text{Bi}_2\text{WO}_6@ \text{g-C}_3\text{N}_4$ samples (Fig. 5) show peak intensities decrease in the following order $\text{g-C}_3\text{N}_4 > 0.5 \text{ wt } \% \text{ Bi}_2\text{WO}_6@ \text{g-C}_3\text{N}_4 > 1.0 \text{ wt } \% \text{ Bi}_2\text{WO}_6@ \text{g-C}_3\text{N}_4 > 1.5 \text{ wt } \% \text{ Bi}_2\text{WO}_6@ \text{g-C}_3\text{N}_4 > 2.0 \text{ wt } \% \text{ Bi}_2\text{WO}_6@ \text{g-C}_3\text{N}_4$.

Table 2
Band gap of $g\text{-C}_3\text{N}_4$ and $\text{Bi}_2\text{WO}_6@g\text{-C}_3\text{N}_4$ samples

Samples	Band gap, eV
$g\text{-C}_3\text{N}_4$	2.43
0.5 wt % $\text{Bi}_2\text{WO}_6@g\text{-C}_3\text{N}_4$	2.27
1.0 wt % $\text{Bi}_2\text{WO}_6@g\text{-C}_3\text{N}_4$	2.25
1.5 wt % $\text{Bi}_2\text{WO}_6@g\text{-C}_3\text{N}_4$	2.02
2.0 wt % $\text{Bi}_2\text{WO}_6@g\text{-C}_3\text{N}_4$	2.01

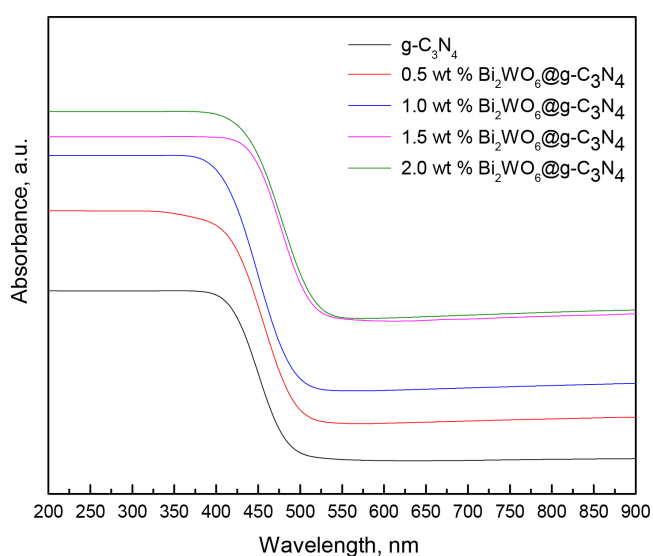


Fig. 4. UV-Vis spectra of $g\text{-C}_3\text{N}_4$, 0.5 wt % $\text{Bi}_2\text{WO}_6@g\text{-C}_3\text{N}_4$, 1.0 wt % $\text{Bi}_2\text{WO}_6@g\text{-C}_3\text{N}_4$, 1.5 wt % $\text{Bi}_2\text{WO}_6@g\text{-C}_3\text{N}_4$ and 2.0 wt % $\text{Bi}_2\text{WO}_6@g\text{-C}_3\text{N}_4$ samples.

$\text{Bi}_2\text{WO}_6@g\text{-C}_3\text{N}_4 > 2.0$ wt % $\text{Bi}_2\text{WO}_6@g\text{-C}_3\text{N}_4$. The values of band gap energy of $g\text{-C}_3\text{N}_4$, 0.5 wt % $\text{Bi}_2\text{WO}_6@g\text{-C}_3\text{N}_4$, 1.0 wt % $\text{Bi}_2\text{WO}_6@g\text{-C}_3\text{N}_4$, 1.5 wt % $\text{Bi}_2\text{WO}_6@g\text{-C}_3\text{N}_4$ and 2.0 wt % $\text{Bi}_2\text{WO}_6@g\text{-C}_3\text{N}_4$ samples calculated from their PL emission spectra were 2.42, 2.26, 2.24, 2.01 and 2.00, respectively, confirming data observed from the UV-Vis spectra.

3.2. Evolution of photo catalytic performance

The type of photo catalyst, dose of 1.5 wt % $\text{Bi}_2\text{WO}_6@g\text{-C}_3\text{N}_4$ photo catalyst, recycling, and reuse of 1.5 wt % $\text{Bi}_2\text{WO}_6@g\text{-C}_3\text{N}_4$ were studied to measure the photo catalytic performance for methanol production under visible light conditions.

The effect of the type of photo catalyst on hydrogen evolution was studied under the following conditions: 500 W Xe lamp light source; 1 h reaction time; 0.4 g/L dose of photo catalyst; 50 mL volume of aqueous solution. Fig. 6 shows the effect of type of photo catalyst on the amount of methanol evolution. The $g\text{-C}_3\text{N}_4$ sample almost has a 0.4 μmol amount of evolved methanol. The performance of 0.5 wt % $\text{Bi}_2\text{WO}_6@g\text{-C}_3\text{N}_4$, 1.0 wt % $\text{Bi}_2\text{WO}_6@g\text{-C}_3\text{N}_4$, 1.5 wt % $\text{Bi}_2\text{WO}_6@g\text{-C}_3\text{N}_4$ and 2.0 wt % $\text{Bi}_2\text{WO}_6@g\text{-C}_3\text{N}_4$ samples for methanol evolution was increased from 0.46° 0.76 μmol , respectively, due to the decreased band gap of 0.5

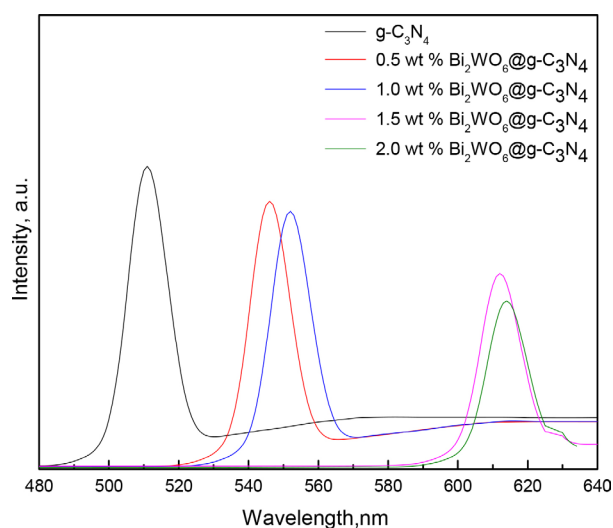


Fig. 5. PL spectra of $g\text{-C}_3\text{N}_4$, 0.5 wt % $\text{Bi}_2\text{WO}_6@g\text{-C}_3\text{N}_4$, 1.0 wt % $\text{Bi}_2\text{WO}_6@g\text{-C}_3\text{N}_4$, 1.5 wt % $\text{Bi}_2\text{WO}_6@g\text{-C}_3\text{N}_4$ and 2.0 wt % $\text{Bi}_2\text{WO}_6@g\text{-C}_3\text{N}_4$ samples.

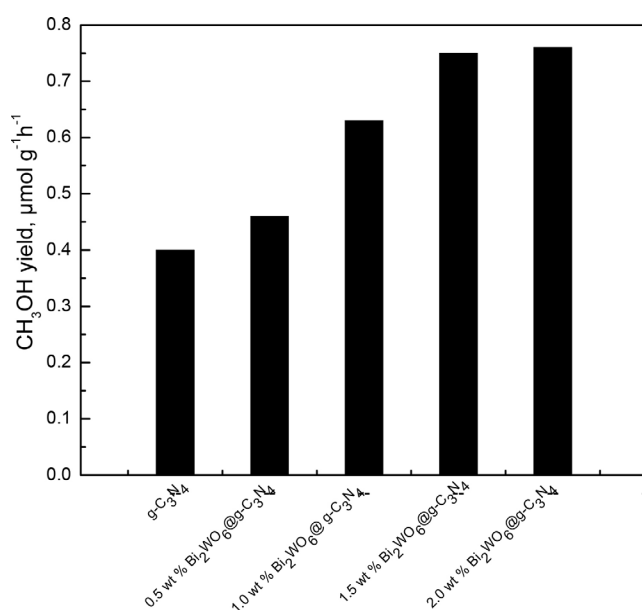


Fig. 6. Effect of the type of photocatalyst on evolved methanol.

wt % $\text{Bi}_2\text{WO}_6@g\text{-C}_3\text{N}_4$, 1.0 wt % $\text{Bi}_2\text{WO}_6@g\text{-C}_3\text{N}_4$, 1.5 wt % $\text{Bi}_2\text{WO}_6@g\text{-C}_3\text{N}_4$ and 2.0 wt % $\text{Bi}_2\text{WO}_6@g\text{-C}_3\text{N}_4$ from 2.27, 2.25, 2.02 and 2.01 eV by Bi_2WO_6 doping.

The effect of dose of 1.5 wt % $\text{Bi}_2\text{WO}_6@g\text{-C}_3\text{N}_4$ photo catalyst on the amount of methanol evolution was studied under the following conditions: 500 W Xe lamp light source; 1 h reaction time; the dose of photo catalyst changed from 0.4 to 2.0 g/L; 50 mL volume of aqueous solution. Fig. 7 shows the effect of dose of 1.5 wt % $\text{Bi}_2\text{WO}_6@g\text{-C}_3\text{N}_4$ photo catalyst on evolved methanol. Methanol evolution increased from 0.75 to 0.90 μmol when the dose of 1.5 wt % $\text{Bi}_2\text{WO}_6@g\text{-C}_3\text{N}_4$ photo catalyst was increased from 0.4 to 1.2 g/L, respectively. This could be explained by the increase in the number of available sites for a photo catalytic reaction as

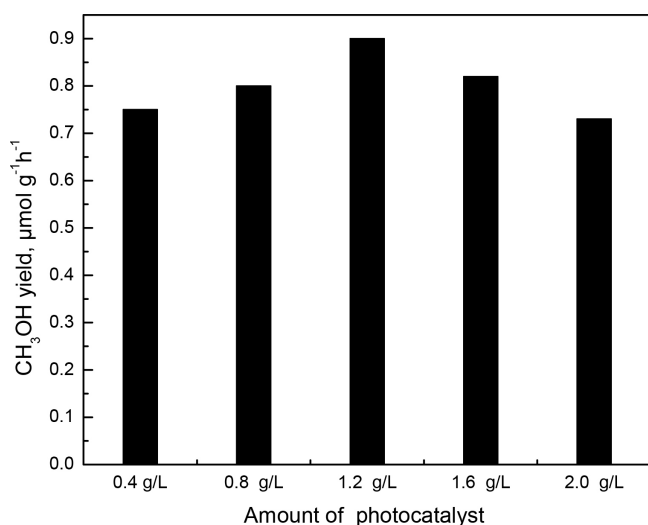


Fig. 7. Effect of the dose of the 1.5 wt % Bi₂WO₆@g-C₃N₄ photocatalyst on evolved methanol.

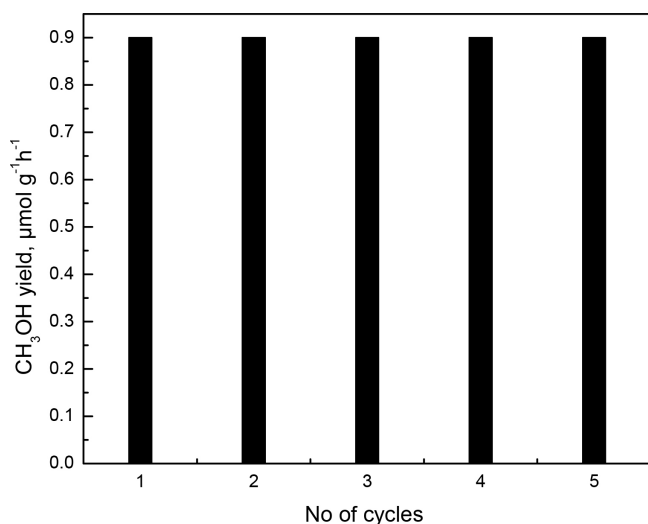


Fig. 8. Recycling and reuse of the 1.5 wt % Bi₂WO₆@g-C₃N₄ photocatalyst on evolved methanol.

the dose increase resulted in more photo catalytic activity. Upon increasing the dose of photo catalyst above 1.2 g/L, the amount of evolved methanol decreases to 0.73 μmol. This may result from the hindrance of light penetration due to the high concentration of photo catalyst particles in the reaction solution.

Recycling and reuse of 1.5 wt % Bi₂WO₆@g-C₃N₄ photo catalyst on evolved methanol was studied under the following conditions: 500 W Xe lamp light source; 1 h reaction time; 1.2 g/L dose of photo catalyst; 50 mL volume of aqueous solution. Fig. 8 shows the recycling and reuse of the 1.5 wt % Bi₂WO₆@g-C₃N₄ photo catalyst on evolved methanol. It is clear that the 1.5 wt % Bi₂WO₆@g-C₃N₄ photo catalyst has photo catalytic stability and can be used and recycled many times.

Visible Light Irradiation

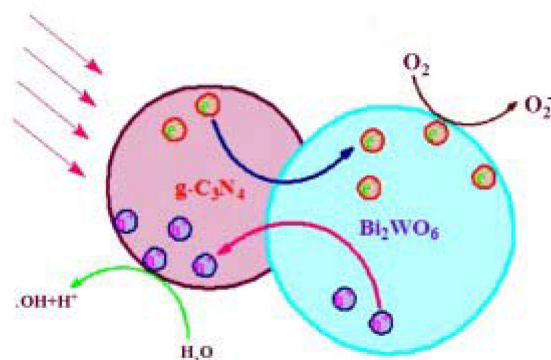
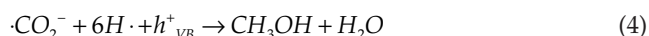


Fig. 9. Photocatalytic mechanism of the 1.5 wt % Bi₂WO₆@g-C₃N₄ photocatalyst.

3.3. The photo catalytic mechanism

The photo catalytic reduction of CO₂ to methanol was shown in Fig. 9 and equations one through four. When the Bi₂WO₆@g-C₃N₄ nanocomposite was irradiated by visible light, the electron-hole pairs were generated on the surface of the Bi₂WO₆@g-C₃N₄ nanocomposite, as shown in Fig. 9. The effect of Bi₂WO₆ in the Bi₂WO₆@g-C₃N₄ nanocomposite is to act as an electron acceptor, thereby hindering the e-h recombination rate. This leads to a carbon dioxide reduction by excited electrons and methanol production as outlined in equations 1 to 4 [22,23].



4. Conclusions

G-C₃N₄ and Bi₂WO₆@g-C₃N₄ were prepared by a hydrothermal method in the presence of octadecyltrimethyl ammonium bromide, which acted as a surfactant. The hydrothermal method in the presence of a surfactant result in the formation of g-C₃N₄ decorated with Bi₂WO₆. A red shift is also observed because of the doping of Bi₂WO₆. The photo catalytic activity of Bi₂WO₆@g-C₃N₄ was 1.9 times better than g-C₃N₄ at methanol production. Bi₂WO₆@g-C₃N₄ shows photo catalytic stability for methanol production even with repeated use.

Acknowledgments

This project was funded by the Deanship of Scientific Research (DSR) at King Abdulaziz University, Jeddah, under grant no.(G-229-130-38). The authors, therefore, acknowledge DSR with thanks for the technical and financial support.

References

- [1] L. Hong, W. Lingzhi, L. Yongdi, L. Juying, Z. Jinlong, Mesoporous graphitic carbon nitride materials: synthesis and modifications, *Res. Chem. Intermed.*, 42 (2016) 3979–3998.
- [2] M. Mousavi, A.H. Yangjeh, Magnetically separable ternary $g\text{-C}_3\text{N}_4/\text{Fe}_3\text{O}_4/\text{BiOI}$ nano composites: Novel visible-light-driven photo catalysts based on graphitic carbon nitride, *J. Colloid. Interface Sci.*, 465 (2016) 83–92.
- [3] A.P. Singh, P. Arora, S. Basu, B.R. Mehta, Graphitic carbon nitride based hydrogen treated disordered titanium dioxide core-shell nano catalyst for enhanced photo catalytic and photo electro chemical performance, 41 (2016) 5617–5628.
- [4] S. Zhou, Y. Liu, J. Li, Y. Wang, G. Jiang, Z. Zhao, D. Wang, A. Duan, J. Liu, Y. Wei, Facile in situ synthesis of graphitic carbon nitride ($g\text{-C}_3\text{N}_4$)- N-TiO_2 hetero junction as an efficient photo catalyst for the selective photo reduction of CO_2 to CO, *Appl. Catal. B.*, 158–159 (2014) 20–29.
- [5] W. Yongmei, T. Li, Z. Jie, Y. Xiu, D. Wenye, L. Yingxuan, W. Chuanyi, $\text{TiO}_2/g\text{-C}_3\text{N}_4$ nano sheets hybrid photo catalyst with enhanced photo catalytic activity under visible light irradiation, *Res. Chem. Inter med.*, 42 (2016) 3609–3624.
- [6] C. Li, H. Wu, L. Zhao, G. Jin, H.Y. XU, $\text{TiO}_2/g\text{-C}_3\text{N}_4$ hetero junctions: In situ fabrication mechanism and enhanced photo catalytic activity, *Front. Mater. Sci.*, 10(3) (2016) 310–319.
- [7] S. Le, T. Jiang, Y. Li, Q. Zhao, Y. Li, W. Fang, M. Gong, Highly efficient visible-light-driven mesoporous graphitic carbon nitride/ ZnO nano composite photo catalysts, *Appl. Catal. B.*, 200 (2017) 601–610.
- [8] B. Xue, H.Y. Jiang, T. Sun, F. Mao, $\text{ZnS}@g\text{-C}_3\text{N}_4$ Composite photo catalysts: in situ synthesis and enhanced visible-light photo catalytic activity, *Catal. Lett.*, 146 (2016) 2185–2192.
- [9] L. Zhang, Q. Zhang, H. Jiu, G. He, Preparation of $g\text{-C}_3\text{N}_4/\text{Zn}_2\text{GeO}_4$ hetero junctions with enhanced photo catalytic activity under visible light, *J. Mater. Sci. Mater. Electron.*, 27 (2016) 7311–7317.
- [10] Y. Zheng, Z. Zhang, C. Li, Beta- FeOOH -supported graphitic carbon nitride as an efficient visible light photo catalyst, *J. Mol. Catal. A. Chem. A.*, 423 (2016) 463–471.
- [11] X. Jia, R. Dai, Y. Sun, H. Song, X. Wu, One-step hydrothermal synthesis of $\text{Fe}_3\text{O}_4/g\text{-C}_3\text{N}_4$ nano composites with improved photo catalytic activities, *J. Mater. Sci. Mater. Electron.*, 27 (2016) 3791–3798.
- [12] K. Katsumata, R. Motoyoshi, N. Matsushita, K. Okada, Preparation of graphitic carbon nitride ($g\text{-C}_3\text{N}_4$)/ WO_3 composites and enhanced visible-light-driven photo degradation of acetaldehyde gas, *J. Haz. Mat.*, 260 (2013) 475–482.
- [13] T. Ohno, N. Murakami, T. Koyanagi, Y. Yang, Photo catalytic reduction of CO_2 over a hybrid photo catalyst composed of WO_3 and graphitic carbon nitride ($g\text{-C}_3\text{N}_4$) under visible light, *J. CO₂ Util.*, 6 (2014) 17–25.
- [14] R. Yin, Q. Luo, D. Wang, H. Sun, Y. Li, X. Li, J. An, $\text{SnO}_2/g\text{-C}_3\text{N}_4$ photo catalyst with enhanced visible-light photo catalytic activity, *J. Mater. Sci.*, 49 (2014) 6067–6073.
- [15] Z. Chengzhang, J. Zhifeng, W. Wei, C. Linlin, L. Dong, Q. Kun, L. Xiaomeng, X. Jimin, Fabrication of noble-metal-free $\text{NiS}_2/g\text{-C}_3\text{N}_4$ hybrid photo catalysts with visible light-responsive photo catalytic activities, *Res. Chem. Inter med.*, 42 (2016) 6483–6499.
- [16] Y. Ming, J. Xiaoqi, Visible light-induced antibacterial and biofilm elimination activity of graphitic carbon nitride by embedded Ag nano particles, *Nano Res.*, 8(5) (2015) 1648–1658.
- [17] C. Han, Y. Wang, Y. Lei, B. Wang, N. Wu, Q. Shi, Q. Li, Visible-light-driven enhanced antibacterial and biofilm elimination activity of graphitic carbon nitride by embedded Ag nano particles, *Nano Res.*, 8(5) (2015) 1648–1658.
- [18] R.M. Mohamed, Synthesis and characterization of $\text{AgCl}@g\text{-C}_3\text{N}_4$ graphitic carbon nitride hybrid materials for the photo catalytic degradation of atrazine, *Ceram. Int.*, 41 (2015) 1197–1204.
- [19] L. Shi, L. Liang, F. Wang, M. Liu, J. Sun, Enhanced visible-light photo catalytic activity and stability over $g\text{-C}_3\text{N}_4/\text{Ag}_2\text{CO}_3$ composites, *J. Mater. Sci.*, 50 (2015) 1718–1727.
- [20] M. Yali, S. Ju, C. Dan, X. Gang, Photo degradation performance of methylene blue aqueous solution on $\text{Ag}/g\text{-C}_3\text{N}_4$ catalyst, *Rare. Metals*, 30 (2011) 276–279.
- [21] Q. Yu, S. Guoc, X. Li, M. Zhang, One-step fabrication and high photo catalytic activity of porous graphitic carbon nitride/graphene oxide hybrid by direct polymerization of cyanamide without templates, *Russ. J. Phys. Chem. A.*, 88 (2014) 1643–1649.
- [22] I. Shown, H.C. Hsu, Y.C. Chang, C.H. Lin, P.K. Roy, A. Ganguly, C.H. Wang, J.K. Chang, C.I. Wu, L.C. Chen, Highly efficient visible light photo catalytic reduction of CO_2 to hydrocarbon fuels by Cu-nano particles decorated graphene oxide, *Nano Lett.*, 14 (2014) 6097–6103.
- [23] E. Karamian, S. Sharifnia, On the general mechanism of photo catalytic reduction of CO_2 , *J. CO₂ Util.*, 16 (2016) 194–203.